Hindawi Publishing Corporation
International Journal of Rotating Machinery
Volume 2008, Article ID 752062, 10 pages
doi:10.1155/2008/752062

Research Article

Free Vibration Analysis of a Rotating Composite Shaft Using the p-Version of the Finite Element Method

A. Boukhalfa, A. Hadjoui, and S. M. Hamza Cherif

Department of Mechanical Engineering, Faculty of Sciences Engineering, Abou Bakr Belkaid University, Tlemcen 13000, Algeria

Correspondence should be addressed to A. Boukhalfa, bka1975e@yahoo.fr

Received 19 November 2007; Accepted 24 May 2008

Recommended by Agnes Muszynska

This paper is concerned with the dynamic behavior of the rotating composite shaft on rigid bearings. A p-version, hierarchical finite element is employed to define the model. A theoretical study allows the establishment of the kinetic energy and the strain energy of the shaft, necessary to the result of the equations of motion. In this model the transverse shear deformation, rotary inertia and gyroscopic effects, as well as the coupling effect due to the lamination of composite layers have been incorporated. A hierarchical beam finite element with six degrees of freedom per node is developed and used to find the natural frequencies of a rotating composite shaft. A program is elaborate for the calculation of the eigenfrequencies and critical speeds of a rotating composite shaft. To verify the present model, the critical speeds of composite shaft systems are compared with those available in the literature. The efficiency and accuracy of the methods employed are discussed.

1. INTRODUCTION

The application of composite shafts has come a long way from early low-speed automotive driveshafts to helicopter tail rotors operating above the second critical speed. With operation at supercritical speeds, a substantial amount of payoffs and net system weight reductions are possible. At the same time, the rotordynamic aspects assume more importance, and detailed analysis is required. There are some technological problems associated with implementation, such as joints with bearings, affixing of lumped masses, couplings, provision of external damping, and so forth. The solutions proposed are just adequate, but require substantial refinements, which might explain some of the differing experiences of various authors.

Zinberg and Symonds [1] described a boron/epoxy composite tail rotor driveshaft for a helicopter. The critical speeds were determined using equivalent modulus beam theory (EMBT), assuming the shaft to be a thin-walled circular tube simply supported at the ends. Shear deformation was not taken into account. The shaft critical speed was determined by extrapolation of the unbalance response curve which was obtained in the subcritical region.

Dos Reis et al. [2] published analytical investigations on thin-walled layered composite cylindrical tubes. In part III of the series of publications, the beam element was extended to formulate the problem of a rotor supported on general eight coefficient bearings. Results were obtained for shaft configuration of Zinberg and Symmonds. The authors have shown that bending-stretching coupling and shear-normal coupling effects change with stacking sequence, and alter the frequency values. Gupta and Singh [3] studied the effect of shear-normal coupling on rotor natural frequencies and modal damping. Kim and Bert [4] have formulated the problem of determination of critical speeds of a composite shaft including the effects of bending-twisting coupling. The shaft was modelled as a Bresse-Timoshenko beam. The shaft gyroscopics have also been included. The results compare well with Zinberg's rotor [1]. In another study, Bert and Kim [5] have analysed the dynamic instability of a composite drive shaft subjected to fluctuating torque and/or rotational speed by using various thin shell theories. The rotational effects include centrifugal and Coriolis forces. Dynamic instability regions for a long span simply supported shaft are presented.

M.-Y. Chang et al. [6] published the vibration behaviours of the rotating composite shafts. In the model, the transverse shear deformation, rotary inertia, and gyroscopic effects, as well as the coupling effect due to the lamination of composite layers have been incorporated. The model based

on a first-order shear deformable beam theory (continuum-based Timoshenko beam theory).

C.-Y. Chang et al. [7] published the vibration analysis of rotating composite shafts containing randomly oriented reinforcements. The Mori-Tanaka mean-field theory is adopted here to account for the interaction at the finite concentrations of reinforcements in the composite material.

Additional recent work on composite shafts dealing with both the theoretical and experimental aspects was reported by Singh [8], Gupta and Singh [3], and Singh and Gupta [9, 10]. Rotordynamic formulation based on equivalent modulus beam theory was developed for a composite rotor with a number of lumped masses and supported on general eight coefficient bearings. A layerwise beam theory was derived by Gupta and Singh [3] from an available shell theory, with a layerwise displacement field, and was then extended to solve a general composite rotordynamic problem. The conventional rotor dynamic parameters as well as critical speeds, natural frequencies, damping factors, unbalance response, and threshold of stability were analysed in detail and results from the formulations based on the two theories, namely, the equivalent modulus beam theory (EMBT) and layerwise beam theory (LBT) were compared [9, 10]. The experimental rotordynamic studies carried by Singh and Gupta [11, 12] were conducted on two filament wound carbon/epoxy shafts with constant winding angles ($\pm 45^\circ$ and $\pm 60^\circ$). Progressive balancing had to be carried out to enable the shaft to traverse through the first critical speed. Inspite of the very different shaft configurations used, the authors' have shown that bending-stretching coupling and shear-normal coupling effects change with stacking sequence, and alter the frequency values.

Some practical aspects such as effect of shaft disc angular misalignment, interaction between shaft bow, which is common in composite shafts and rotor unbalance, and an unsuccessful operation of a composite rotor with an external damper were discussed and reported by Singh and Gupta [11]. The Bode and cascade plots were generated and orbital analysis at various operating speeds was performed. The experimental critical speeds showed good correlation with the theoretical prediction.

This paper deals with the p-version, hierarchical finite element method applied to free vibration analysis of rotating composite shafts. The hierarchical concept for finite element shape functions has been investigated during the past 25 years. Babuska et al. [13] established a theoretical basis for p-elements, where the mesh keeps unchanged and the polynomial degree of the shape functions is increased; however, in the standard h-version of the finite element method the mesh is refined to achieve convergence and the polynomial degree of the shape functions remains unchanged. Since then, standard forms of the hierarchical shape functions have been represented in the literature elsewhere; see for instance [14, 15].

Meirovitch and Baruh [16] and Zhu [17] have shown that the hierarchical finite element method yields a better accuracy than the h-version for eigenvalues problems. The hierarchical shape functions used by Bardell [18] are based on integrated Legendre orthogonal polynomials; the symbolic computing is used to calculate the mass and stiffness matrices of beams and plates. Côté and Charron [19] give the selection of p-version shape functions for plate vibration analysis.

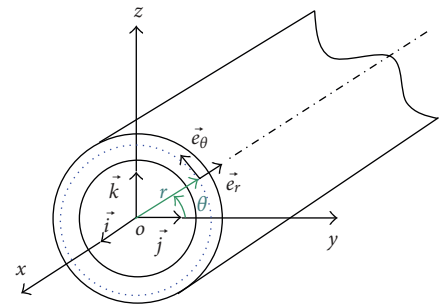

Figure 1: The cylindrical coordinate system.

In the presented composite shaft model, the Timoshenko theory will be adopted. It is the purpose of the present work to study dynamic characteristics such as natural frequencies, whirling frequencies, and the critical speeds of the rotating composite shaft. In the model, the transverse shear deformation, rotary inertia, and gyroscopic effects, as well as the coupling effect due to the lamination of composite layers have been incorporated. To determine the rotating shaft system's responses, the hierarchical finite element method with trigonometric shape functions [20, 21] is used here to approximate the governing equations by a system of ordinary differential equations.

2. EQUATIONS OF MOTION

2.1. Kinetic and strain energy expressions

The shaft is modelled as a Timoshenko beam, that is, first-order shear deformation theory with rotary inertia and gyroscopic effect is used. The shaft rotates at constant speed about its longitudinal axis. Due to the presence of fibers oriented than axially or circumferentially, coupling is made between bending and twisting. The shaft has a uniform, circular cross-section.

The following displacement field of a rotating shaft is assumed by choosing the coordinate axis x to coincide with the shaft axis:

$$\begin{aligned} U(x,y,z,t) &= U_0(x,t) + z\beta_x(x,t) - y\beta_y(x,t), \\ V(x,y,z,t) &= V_0(x,t) - z\phi(x,t), \\ W(x,y,z,t) &= W_0(x,t) + y\phi(x,t), \end{aligned} \tag{1}$$

where U, V, and W are the flexural displacements of any point on the cross-section of the shaft in the x, y, and z directions (see Figure 1), the variables U_0, V_0, and W_0 are the flexural displacements of the shaft's axis, while β_x and β_y are the rotation angles of the cross-section, about the y and z axis, respectively. The ϕ is the angular displacement of the cross-section due to the torsion deformation of the shaft.

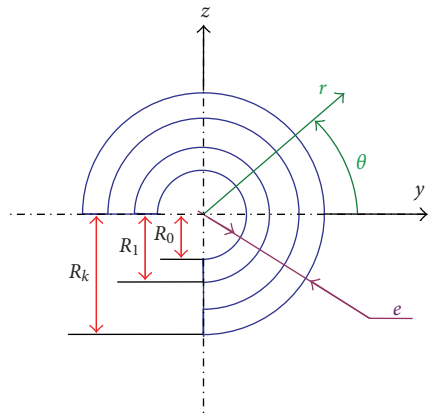

Figure 2: k-layers of composite shaft.

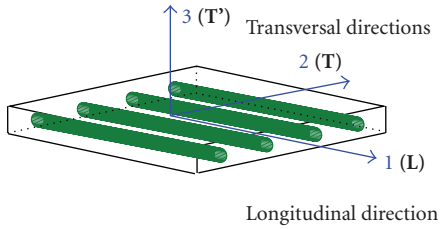

Figure 3: A typical composite lamina and its principal axes.

The strain components in the cylindrical coordinate system (as shown in Figures 1-2) can be written in terms of the displacement variables defined earlier as

$$\begin{aligned}
\varepsilon_{xx} &= \frac{\partial U_0}{\partial x} + r\sin\theta\frac{\partial \beta_x}{\partial x} - r\cos\theta\frac{\partial \beta_y}{\partial x},\\
\varepsilon_{rr} &= \varepsilon_{\theta\theta} = \varepsilon_{r\theta} = 0,\\
\varepsilon_{x\theta} &= \varepsilon_{\theta x}\\
&= \frac{1}{2}\left(\beta_y\sin\theta + \beta_x\cos\theta - \sin\theta\frac{\partial V_0}{\partial x} + \cos\theta\frac{\partial W_0}{\partial x} + r\frac{\partial \phi}{\partial x}\right),\\
\varepsilon_{xr} &= \varepsilon_{rx}\\
&= \frac{1}{2}\left(\beta_x\sin\theta - \beta_y\cos\theta - \sin\theta\frac{\partial W_0}{\partial x} + \cos\theta\frac{\partial V_0}{\partial x}\right).
\end{aligned} \tag{2}$$

Let us consider a composite shaft consists of k layered (Figure 2) of fiber inclusion reinforced laminate. The constitutive relations for each layer are described by

$$\begin{Bmatrix}\sigma_{xx}\\ \sigma_{\theta\theta}\\ \sigma_{rr}\\ \tau_{r\theta}\\ \tau_{xr}\\ \tau_{x\theta}\end{Bmatrix} = \begin{bmatrix} C'_{11} & C'_{12} & C'_{13} & 0 & 0 & C'_{16}\\ C'_{12} & C'_{22} & C'_{23} & 0 & 0 & C'_{26}\\ C'_{13} & C'_{23} & C'_{33} & 0 & 0 & C'_{36}\\ 0 & 0 & 0 & C'_{44} & C'_{45} & 0\\ 0 & 0 & 0 & C'_{45} & C'_{55} & 0\\ C'_{16} & C'_{26} & C'_{36} & 0 & 0 & C'_{66}\end{bmatrix}\begin{Bmatrix}\varepsilon_{xx}\\ \varepsilon_{\theta\theta}\\ \varepsilon_{rr}\\ \gamma_{r\theta}\\ \gamma_{xr}\\ \gamma_{x\theta}\end{Bmatrix}, \tag{3}$$

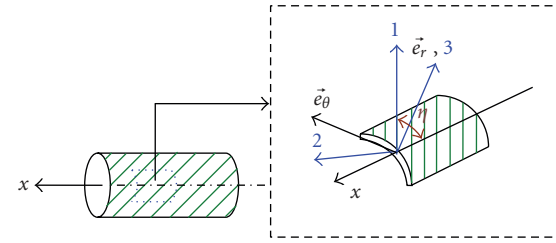

Figure 4: The definitions of the principal coordinate axes on an arbitrary layer of the composite.

where C'_{ij} are the effective elastic constants, they are related to lamination angle η (as shown in Figures 3-4) and the elastic constants of principal axes.

The stress-strain relations of the nth layer expressed in the cylindrical coordinate system (Figure 5) can be expressed as

$$\begin{aligned}
\sigma_{xx} &= C'_{11n}\varepsilon_{xx} + k_s C'_{16n}\gamma_{x\theta},\\
\tau_{x\theta} &= \tau_{\theta x} = k_s C'_{16n}\varepsilon_{xx} + k_s C'_{66n}\gamma_{x\theta},\\
\tau_{xr} &= \tau_{rx} = k_s C'_{55n}\gamma_{xr},
\end{aligned} \tag{4}$$

where k_s is the transverse shear correction factor.

The formula of the strain energy is

$$E_d = \frac{1}{2}\int_V \left(\sigma_{xx}\varepsilon_{xx} + 2\tau_{xr}\varepsilon_{xr} + 2\tau_{x\theta}\varepsilon_{x\theta}\right) dV. \tag{5}$$

The various components of strain energy come from the shaft:

$$\begin{aligned}
E_d &= \frac{1}{2}A_{11}\int_0^L\left(\frac{\partial U_0}{\partial x}\right)^2 dx\\
&\quad + \frac{1}{2}B_{11}\left[\int_0^L\left(\frac{\partial \beta_x}{\partial x}\right)^2 dx + \int_0^L\left(\frac{\partial \beta_y}{\partial x}\right)^2 dx\right]\\
&\quad + \frac{1}{2}k_s B_{66}\int_0^L\left(\frac{\partial \phi}{\partial x}\right)^2 dx + \frac{1}{2}k_s A_{16}\\
&\quad \times\left[2\int_0^L\frac{\partial \phi}{\partial x}\frac{\partial U_0}{\partial x}dx + \int_0^L\beta_y\frac{\partial \beta_x}{\partial x}dx - \int_0^L\beta_x\frac{\partial \beta_y}{\partial x}dx\right.\\
&\qquad \left. - \int_0^L\frac{\partial V_0}{\partial x}\frac{\partial \beta_x}{\partial x}dx - \int_0^L\frac{\partial W_0}{\partial x}\frac{\partial \beta_y}{\partial x}dx\right]\\
&\quad + \frac{1}{2}k_s(A_{55} + A_{66})\\
&\quad \times\left[\int_0^L\left(\frac{\partial V_0}{\partial x}\right)^2 dx + \int_0^L\left(\frac{\partial W_0}{\partial x}\right)^2 dx + \int_0^L\beta_x^2 dx\right.\\
&\qquad \left. + \int_0^L\beta_y^2 dx + 2\int_0^L\beta_x\frac{\partial W_0}{\partial x}dx - 2\int_0^L\beta_y\frac{\partial V_0}{\partial x}dx\right],
\end{aligned} \tag{6}$$

where A_{ij} and B_{ij} are given in the appendix.

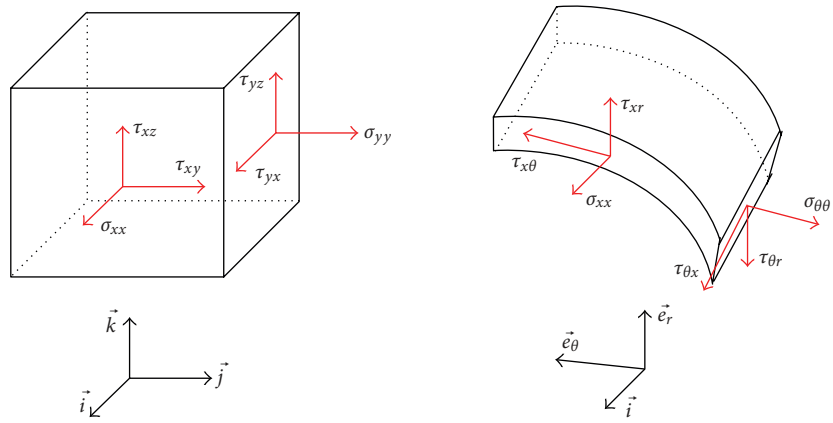

Figure 5: The stress components: (a) in the coordinate axes (x, y, z), (b) in the coordinate axes (x, r, θ).

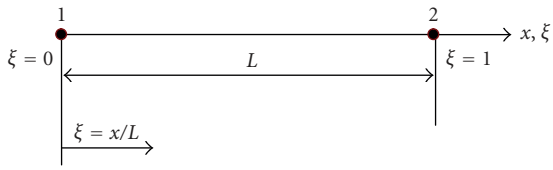

Figure 6: Beam element with two nodes.

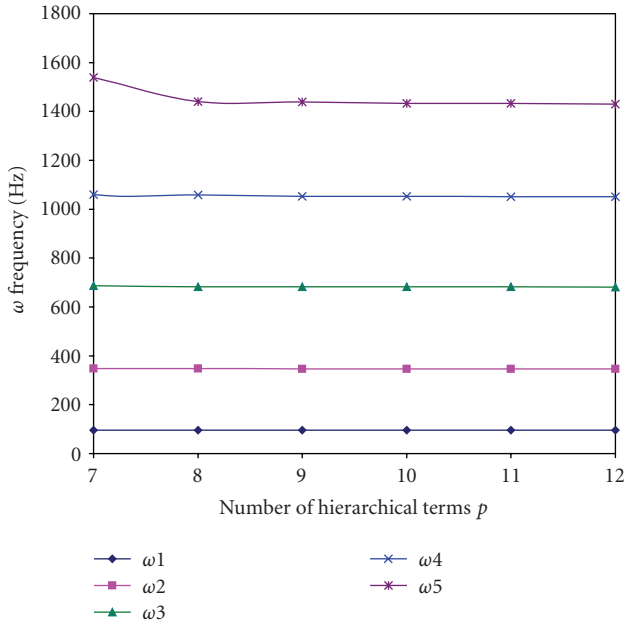

Figure 7: Convergence of the frequency ω for the 5 bending modes of the simply-supported (S-S) shaft as a function of the number of hierarchical terms p.

The kinetic energy of the rotating composite shaft, including the effects of translatory and rotary inertia, can be

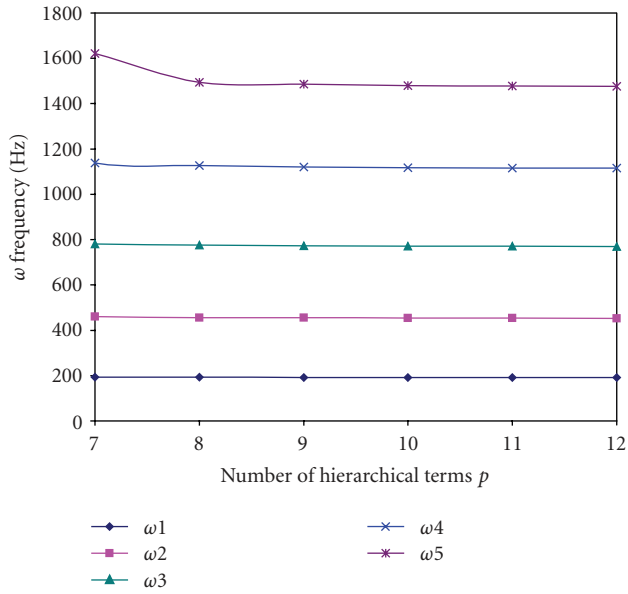

Figure 8: Convergence of the frequency ω for the 5 bending modes of the clamped-clamped (C-C) shaft as a function of the number of hierarchical terms p.

written as

$$E_c = \frac{1}{2}\int_0^L [I_m(\dot{U}_0^2 + \dot{V}_0^2 + \dot{W}_0^2) + I_d(\dot{\beta}_x^2 + \dot{\beta}_y^2) - 2\Omega I_p \beta_x \dot{\beta}_y + 2\Omega I_p \dot{\phi} + I_p \dot{\phi}^2 + \Omega^2 I_p + \Omega^2 I_d(\beta_x^2 + \beta_y^2)]\, dx, \tag{7}$$

where Ω is the rotating speed of the shaft which is assumed constant, L is the length of the shaft, the $2\Omega I_p \beta_x \dot{\beta}_y$ term accounts for the gyroscopic effect, and $I_d(\dot{\beta}_x^2 + \dot{\beta}_y^2)$ represent the rotary inertia effect. The mass moments of inertia I_m, the diametrical mass moments of inertia I_d, and polar mass moment of inertia I_p of rotating shaft per unit length are defined in the appendix. As the $\Omega^2 I_d(\beta_x^2 + \beta_y^2)$ term is far smaller than $\Omega^2 I_p$, it will neglected in further analysis.

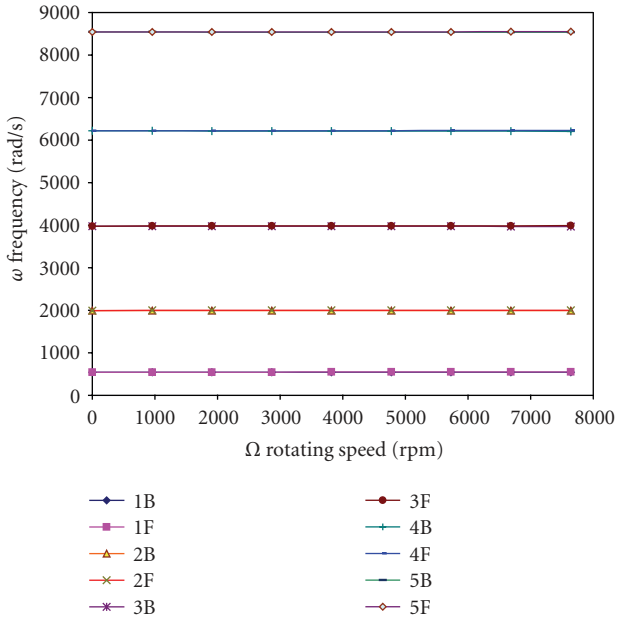

Figure 9: The Campbell diagram of a composite shaft ((F) forward modes, (B) backward modes).

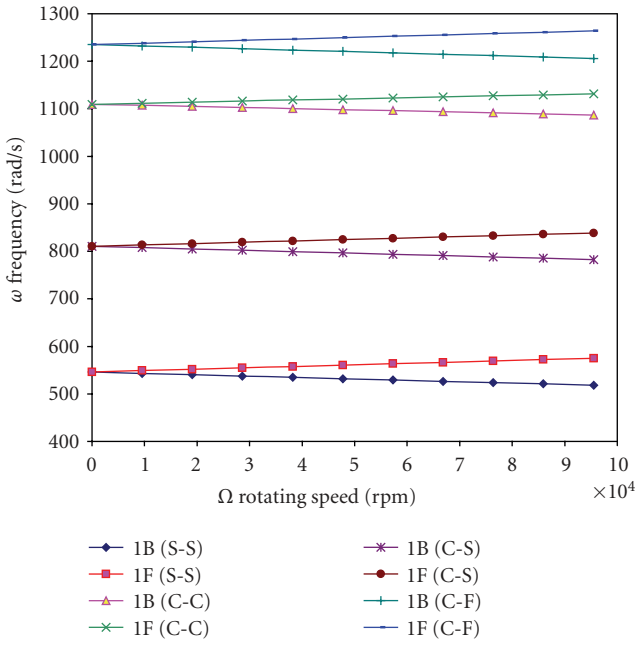

Figure 10: The first backward (1B) and forward (1F) bending mode of a composite shaft for different boundary conditions and different rotating speeds (S: simply supported; C: clamped; F: free).

2.2. Hierarchical beam element formulation

The spinning flexible beam is descretised into one hierarchical finite element is shown in Figure 6. The element's nodal d.o.f. at each node are U_0, V_0, W_0, β_x, β_y, and ϕ. The local and nondimensional coordinates are related by

$$\xi = x/L, \quad (0 \le \xi \le 1). \tag{8}$$

Table 1: Properties of composite materials [22].

	Boron-epoxy	Graphite-epoxy
E_{11} (GPa)	211.0	139.0
E_{22} (GPa)	24.1	11.0
G_{12} (GPa)	6.9	6.05
G_{23} (GPa)	6.9	3.78
ν_{12}	0.36	0.313
ρ (kg/m^3)	1967.0	1578.0

The vector displacement formed by the variables U_0, V_0, W_0, β_x, β_y, and ϕ can be written as

$$\begin{aligned}
U_0 &= \sum_{m=1}^{p_U} x_m(t)\cdot f_m(\xi),\\
V_0 &= \sum_{m=1}^{p_V} y_m(t)\cdot f_m(\xi),\\
W_0 &= \sum_{m=1}^{p_W} z_m(t)\cdot f_m(\xi),\\
\beta_x &= \sum_{m=1}^{p_{\beta x}} \beta_{xm}(t)\cdot f_m(\xi),\\
\beta_y &= \sum_{m=1}^{p_{\beta y}} \beta_{ym}(t)\cdot f_m(\xi),\\
\phi &= \sum_{m=1}^{p_\phi} \phi_m(t)\cdot f_m(\xi).
\end{aligned} \tag{9}$$

And it can be expressed as

$$\begin{Bmatrix} U_0 \\ V_0 \\ W_0 \\ \beta_x \\ \beta_y \\ \phi \end{Bmatrix} = [N]\{q\}, \tag{10}$$

where $[N]$ is the matrix of the shape functions, given by

$$[N] = \begin{bmatrix} [N_U] & 0 & 0 & 0 & 0 & 0 \\ 0 & [N_V] & 0 & 0 & 0 & 0 \\ 0 & 0 & [N_W] & 0 & 0 & 0 \\ 0 & 0 & 0 & [N_{\beta_x}] & 0 & 0 \\ 0 & 0 & 0 & 0 & [N_{\beta_y}] & 0 \\ 0 & 0 & 0 & 0 & 0 & [N_\phi] \end{bmatrix}, \tag{11}$$

$$[N_{U,V,V,\beta_x,\beta_y,\phi}] = [f_1 f_2 \cdots f_{p_U,p_V,p_W,p_{\beta_x},p_{\beta_y},p_\phi}], \tag{12}$$

where p_U, p_V, p_W, p_{β_x}, p_{β_y}, and p_ϕ are the numbers of hierarchical terms of displacements (are the numbers of shape functions of displacements).

In this work, $p_U = p_V = p_W = p_{\beta_x} = p_{\beta_y} = p_\phi = p$.

Table 2: The critical speed of the boron-epoxy composite shaft.

$L = 2.47$ m, $D = 12.69$ cm, $e = 1.321$ mm, 10 layers of equal thickness (90°, 45°, −45°, $0°_6$, 90°), $k_s = 0.503$		
	Theory or method	First critical speed (rpm)
Zinberg and Symonds [1]	Measured experimentally	6000
	EMBT	5780
dos Reis et al. [2]	Bernoulli-Euler beam theory with stiffness determined by shell finite elements	4942
Kim and Bert [4]	Sanders shell theory	5872
Bert [23]	Donnell shallow shell theory	6399
Bert and Kim [22]	Bernoulli-Euler beam theory	5919
Gupta and Singh [3]	Bresse-Timoshenko beam theory	5788
	EMBT	5747
	LBT	5620
M.-Y. Chang et al. [6]	Continuum-based Timoshenko beam theory	5762
Present	Timoshenko beam theory by the p-version of the finite element method	5760

The vector of generalised coordinates given by

$$\{q\} = \{q_U, q_V, q_W, q_{\beta_x}, q_{\beta_y}, q_\phi\}^T, \tag{13}$$

where

$$\begin{aligned}
\{q_U\} &= \{x_1, x_2, x_3, \ldots, x_{p_U}\}^T \exp(j\omega t),\\
\{q_V\} &= \{y_1, y_2, y_3, \ldots, y_{p_V}\}^T \exp(j\omega t),\\
\{q_W\} &= \{z_1, z_2, z_3, \ldots, y_{p_W}\}^T \exp(j\omega t),\\
\{q_{\beta_x}\} &= \{\beta_{x_1}, \beta_{x_2}, \beta_{x_3}, \ldots, \beta_{x_{P_{\beta_x}}}\}^T \exp(j\omega t),\\
\{q_{\beta_y}\} &= \{\beta_{y_1}, \beta_{y_2}, \beta_{y_3}, \ldots, \beta_{y_{P_{\beta_y}}}\}^T \exp(j\omega t),\\
\{q_\phi\} &= \{\phi_1, \phi_2, \phi_3, \ldots, \phi_{p_\phi}\}^T \exp(j\omega t).
\end{aligned} \tag{14}$$

The group of the shape functions used in this study is given by

$$\begin{aligned}
f_1 &= 1 - \xi,\\
f_2 &= \xi,\\
f_{r+2} &= \sin(\delta_r \xi),\\
\delta_r &= r\pi; \quad r = 1, 2, 3, \ldots.
\end{aligned} \tag{15}$$

The functions (f_1, f_2) are those of the finite element method necessary to describe the nodal displacements of the element, whereas the trigonometric functions f_{r+2} contribute only to the internal field of displacement and do not affect nodal displacements. The most attractive particularity of the trigonometric functions is that they offer great numerical stability. The shaft is modeled by only one element called hierarchical finite element.

By applying the Euler-Lagrange equations, the equations of motion of free vibration of spinning flexible shaft can be obtained:

$$[M]\{\ddot{q}\} + [G]\{\dot{q}\} + [K]\{q\} = \{0\}. \tag{16}$$

The system obtained is linear of which equations are coupled once by the gyroscopic effect, represented by the matrix $[G]$.

$[M]$ and $[K]$ are the conventional hierarchical finite element mass and stiffness matrix, $[G]$ is the gyroscopic matrix (the different matrices of the system of equation are given in the appendix).

3. RESULTS

A program based on the formulation proposed was developed for the resolution of (16).

3.1. Convergence

First, the material properties for boron-epoxy are listed in Table 1, and the geometric parameters are $L = 2.47$ m, $D = 12.69$ cm, $e = 1.321$ mm, 10 layers of equal thickness (90°, 45°, −45°, $0°_6$, 90°). The shear correction factor $k_s = 0.503$ and the rotating speed $\Omega = 0$.

The results of the five bending modes for various boundary conditions of the composite shaft as a function of the number of hierarchical terms are shown in Figures 7 and 8. Figures clearly show that rapid convergence from above to the exact values occur as the number of hierarchical terms is increased.

3.2. Numerical examples and discussions

In all the following examples, $p = 10$.

In the first example, the properties of the boron-epoxy composite shaft are given by Table 1. The results obtained

Table 3: The critical speed of the graphite-epoxy composite shaft.

$L = 2.47$ m, $D = 12.69$ cm, $e = 1.321$ mm, 10 layers of equal thickness $(90^\circ, 45^\circ, -45^\circ, 0^\circ_6, 90^\circ)$, $k_s = 0.503$		
	Theory or method	First critical speed (rpm)
Bert and Kim [22]	Sanders shell theory	5349
	Donnell shallow shell theory	5805
	Bernoulli-Euler beam theory	5302
	Bresse-Timoshenko beam theory	5113
M.-Y. Chang et al. [6]	Continuum-based Timoshenko beam theory	5197
Present	Timoshenko beam theory by the p-version of the finite element method	5200

Table 4: The critical speed (rpm) of the graphite-epoxy composite shaft for various lengths to mean diameter ratio.

Theory or method		L/D							
		2	5	10	15	20	25	30	35
Bert and Kim [22]	Sanders shell	112400	41680	16450	8585	5183	3441	2440	1816
	Bernoulli-Euler	329600	76820	20210	9072	5121	3283	2282	1677
	Bresse-Timoshenko	176300	54830	17880	8543	4945	3209	2246	1658
M.-Y. Chang et al. [6]	Continuum-based Timoshenko beam theory	181996	55706	17929	8527	4925	3192	2233	1648
Present	Timoshenko beam theory by the p-version of the finite element method	184667	56196	18005	8549	4934	3198	2236	1650

using the present model are shown in Table 2 together with those of referenced papers. As can be seen from the table, our results are close to those predicted by other beam theories. Since in the studied example the wall of the shaft is relatively thin, models based on shell theories [4] are expected to yield more accurate results. In the present example, the critical speed measured from the experiment however is still underestimated by using Sander shell theory, while overestimated by Donnell shallow shell theory. When the material of the shaft is changed to the graphite-epoxy given in Table 1 with other conditions left unchanged, the critical speed obtained from the present model is shown in Table 3. In this case, the result from the present model is compatible to that of the Bresse-Timoshenko beam theory of M.-Y. Chang et al. [6].

Next, comparisons are made with those of [6, 22] for different length to mean diameter ratios L/D. The shafts being analysed are made of the graphite-epoxy material given in Table 1 and all have the same lamination $[90^\circ/45^\circ/45^\circ/0^\circ_6/90^\circ]$. The mean diameter and the wall thickness of the shaft remain the same as the previous examples. The shear correction factor being used is again 0.503. The results are listed in Table 4. Further results being compared are for generalized orthotropic composite tube of different lamination angles η. The results are shown in Table 5.

In our work, the shaft is modelled by only one element with two nodes, but in the model of [6] the shaft is modelled by 20 finite elements of equal length (h-version). The rapid convergence while taking only one element and a reduced number of shape functions shows the advantage of the method used.

From the thin-walled shaft systems studied above, the present shaft model yields result in all cases close to those of the model of Bert and Kim [22] based on the Bresse-Timoshenko theory. One should stress here that the present model is not only applicable to the thin-walled composite shafts as studied above, but also to the thick-walled shafts as well as to the solid ones.

In the following example, the frequencies responses of a graphite-epoxy composite shaft system are analysed. The material properties are those listed in Table 1. The lamination scheme of the shaft remains the same as previous examples, while its geometric properties, the Campbell diagram containing the frequencies of the first five pairs of bending whirling modes of the above composite system is shown in Figure 9. The intersection point of the line ($\Omega = \omega$) with the whirling frequency curves indicate the speed at which the shaft will vibrate violently (i.e., the critical speed). The first 10 eigenvalues correspond to 5 forward (F) and 5 backward (B) whirling bending modes of the shaft.

The gyroscopic effect causes a coupling of orthogonal displacements to the axis of rotation, and by consequence separates the frequencies in two branches: backward precession mode and forward precession mode. In all cases, the backward modes increase with increasing rotating speed however the forward modes decrease.

Table 5: The critical speed (rpm) of the graphite-epoxy composite shaft for various lamination angles.

Theory or method		Lamination angle η (°)						
		0	15	30	45	60	75	90
Bert and Kim [22]	Sanders shell	5527	4365	3308	2386	2120	2020	1997
	Bernoulli-Euler	6425	5393	4269	3171	2292	1885	1813
	Bresse-Timoshenko	6072	5209	4197	3143	2278	1874	1803
M.-Y. Chang et al. [6]	Continuum-based Timoshenko beam theory	6072	5331	4206	3124	2284	1890	1816
Present	Timoshenko beam theory by the p-version of the finite element method	6094	5359	4222	3129	2284	1890	1816

Figure 10 shows the variation of the bending fundamental frequency ω as a function of the rotating speed Ω (Campbell diagram) for different boundary conditions and different rotating speeds.

The gyroscopic effect inherent to rotating structures induces a precession motion. The backward precession modes (1B) increase with increasing the rotating speed, however the forward precession (1F) modes decrease.

4. CONCLUSION

This paper has presented the free vibration analysis of spinning composite shaft using the p-version, hierarchical finite element method with trigonometric shape functions. Results obtained using the method has been evaluated against those available in the literature and the agreement has been found to be good. The main conclusions have emerged from this work, these are itemised below.

(1) Monotonic and uniform convergence is found to occur as the number of hierarchical functions is increased.

(2) The dynamic characteristics of rotating composite shaft are influenced significantly by varying the fiber orientation, the rotating speed, and boundary conditions.

(3) The gyroscopic effect causes a coupling of orthogonal displacements to the axis of rotation, and by consequence separates the frequencies in two branches: backward and forward precession modes. In all cases, the backward modes increase with increasing rotating speed however the forward modes decrease.

APPENDIX

The terms A_{ij}, B_{ij} of (6) and I_m, I_d, I_p of (7) are given as follows:

$$
\begin{aligned}
A_{11} &= \pi \sum_{n=1}^{k} C'_{11n}(R_n^2 - R_{n-1}^2),\\
A_{55} &= \frac{\pi}{2} \sum_{n=1}^{k} C'_{55n}(R_n^2 - R_{n-1}^2),\\
A_{66} &= \frac{\pi}{2} \sum_{n=1}^{k} C'_{66n}(R_n^2 - R_{n-1}^2),\\
A_{16} &= \frac{2\pi}{3} \sum_{n=1}^{k} C'_{16n}(R_n^3 - R_{n-1}^3),\\
B_{11} &= \frac{\pi}{4} \sum_{n=1}^{k} C'_{11n}(R_n^4 - R_{n-1}^4),\\
B_{66} &= \frac{\pi}{2} \sum_{n=1}^{k} C'_{66n}(R_n^4 - R_{n-1}^4),\\
I_m &= \pi \sum_{n=1}^{k} \rho_n(R_n^2 - R_{n-1}^2),\\
I_d &= \frac{\pi}{4} \sum_{n=1}^{k} \rho_n(R_n^4 - R_{n-1}^4),\\
I_p &= \frac{\pi}{2} \sum_{n=1}^{k} \rho_n(R_n^4 - R_{n-1}^4),
\end{aligned}
\tag{A.1}
$$

where k is the number of the layer, R_{n-1} is the nth layer inner radius of the composite shaft, and R_n is the nth layer outer of the composite shaft. L is the length of the composite shaft and ρ_n is the density of the nth layer of the composite shaft.

Whereas the various matrices of (16) are expressed as follows:

$$
[M] = \begin{bmatrix}
[M_U] & 0 & 0 & 0 & 0 & 0\\
0 & [M_V] & 0 & 0 & 0 & 0\\
0 & 0 & [M_W] & 0 & 0 & 0\\
0 & 0 & 0 & [M_{\beta_x}] & 0 & 0\\
0 & 0 & 0 & 0 & [M_{\beta_y}] & 0\\
0 & 0 & 0 & 0 & 0 & [M_\phi]
\end{bmatrix},
$$

$$
[K] = \begin{bmatrix}
[K_U] & 0 & 0 & 0 & 0 & [K_1]\\
0 & [K_V] & 0 & [K_2] & [K_3] & 0\\
0 & 0 & [K_W] & [K_4] & [K_5] & 0\\
0 & [K_2]^T & [K_4]^T & [K_{\beta_x}] & [K_6] & 0\\
0 & [K_3]^T & [K_5]^T & [K_6]^T & [K_{\beta_y}] & 0\\
[K_1]^T & 0 & 0 & 0 & 0 & [K_\phi]
\end{bmatrix},
$$

$$[G] = \begin{bmatrix} 0 & 0 & 0 & 0 & 0 & 0 \\ 0 & 0 & 0 & 0 & 0 & 0 \\ 0 & 0 & 0 & 0 & 0 & 0 \\ 0 & 0 & 0 & 0 & [G_1] & 0 \\ 0 & 0 & 0 & -[G_1]^T & 0 & 0 \\ 0 & 0 & 0 & 0 & 0 & 0 \end{bmatrix},$$

$$[M_U] = I_m L \int_0^1 [N_U]^T [N_U]\, d\xi,$$

$$[M_V] = I_m L \int_0^1 [N_V]^T [N_V]\, d\xi,$$

$$[M_W] = I_m L \int_0^1 [N_W]^T [N_W]\, d\xi,$$

$$[M_{\beta_x}] = I_d L \int_0^1 [N_{\beta_x}]^T [N_{\beta_x}]\, d\xi,$$

$$[M_{\beta_y}] = I_d L \int_0^1 [N_{\beta_y}]^T [N_{\beta_y}]\, d\xi,$$

$$[M_\phi] = I_p L \int_0^1 [N_\phi]^T [N_\phi]\, d\xi,$$

$$[K_U] = \frac{1}{L} A_{11} \int_0^1 [N'_U]^T [N'_U]\, d\xi,$$

$$[K_V] = \frac{1}{L} k_s (A_{55} + A_{66}) \int_0^1 [N'_V]^T [N'_V]\, d\xi,$$

$$[K_W] = \frac{1}{L} k_s (A_{55} + A_{66}) \int_0^1 [N'_W]^T [N'_W]\, d\xi,$$

$$[K_1] = \frac{1}{L} k_s A_{16} \int_0^1 [N'_\phi]^T [N'_U]\, d\xi,$$

$$[K_2] = -\frac{1}{2L} k_s A_{16} \int_0^1 [N'_V]^T [N'_{\beta_x}]\, d\xi,$$

$$[K_3] = -k_s (A_{55} + A_{66}) \int_0^1 [N_{\beta_y}]^T [N'_V]\, d\xi,$$

$$[K_4] = k_s (A_{55} + A_{66}) \int_0^1 [N_{\beta_x}]^T [N'_W]\, d\xi,$$

$$[K_5] = -\frac{1}{2L} k_s A_{16} \int_0^1 [N'_W]^T [N'_{\beta_y}]\, d\xi,$$

$$[K_6] = \left[\frac{1}{2} k_s A_{16} \int_0^1 [N_{\beta_y}]^T [N'_{\beta_x}]\, d\xi \right] - \left[\frac{1}{2} k_s A_{16} \int_0^1 [N_{\beta_x}]^T [N'_{\beta_y}]\, d\xi \right],$$

$$[K_{\beta_x}] = \left[\frac{1}{L} B_{11} \int_0^1 [N'_{\beta_x}]^T [N'_{\beta_x}]\, d\xi \right] + \left[L k_s (A_{55} + A_{66}) \int_0^1 [N_{\beta_x}]^T [N_{\beta_x}]\, d\xi \right],$$

$$[K_{\beta_y}] = \left[\frac{1}{L} B_{11} \int_0^1 [N'_{\beta_y}]^T [N'_{\beta_y}]\, d\xi \right] + \left[L k_s (A_{55} + A_{66}) \int_0^1 [N_{\beta_y}]^T [N_{\beta_y}]\, d\xi \right],$$

$$[K_\phi] = \frac{1}{L} B_{66} \int_0^1 [N'_\phi]^T [N'_\phi]\, d\xi,$$

$$[G_1] = \Omega I_p L \int_0^1 [N_{\beta_x}]^T [N_{\beta_y}]\, d\xi, \tag{A.2}$$

where $[N'_i] = \partial [N_i]/\partial \xi$, with $(i = U, V, W, \beta_x, \beta_y, \phi)$.

The terms of the matrices are a function of the integrals, $J_{mn}^{\alpha\beta} = \int_0^1 f_m^\alpha(\xi) f_n^\beta(\xi) d\xi$, (m, n) indicate the number of the shape functions used, where (α, β) is the order of derivation.

NOMENCLATURE

$U(x, y, z)$:	Displacement in x direction
$V(x, y, z)$:	Displacement in y direction
$W(x, y, z)$:	Displacement in z direction
β_x:	Rotation angles of the cross-section on y axis
β_y:	Rotation angles of the cross-section on z axis
ϕ:	Angular displacement of the cross-section due to the torsion deformation of the shaft
(x, y, z):	Cartesian coordinates
$(\vec{i}, \vec{j}, \vec{k})$:	Axes of the Cartesian coordinates
(x, r, θ):	Cylindrical coordinates
$(\vec{i}, \vec{e}_r, \vec{e}_\theta)$:	Axes of the cylindrical coordinates
(1, 2, 3):	Principal axes of a layer of laminate
C'_{ij}:	Elastic constants
E:	Young modulus
G:	Shear modulus
ν:	Poisson coefficient
ρ:	Masse density
k_s:	Shear correction factor
L:	Length of the shaft
D:	Mean radius of the shaft
e:	Wall thickness of the shaft
k:	Number of the layer of the composite shaft
R_{n-1}:	The nth layer inner radius of the composite shaft
R_n:	The nth layer outer radius of the composite shaft
R_0:	Inner radius of the composite shaft
R_k:	Outer radius of the composite shaft
η:	Lamination angle
θ:	Circumferential coordinate
ξ:	Local and nondimensional coordinates
ε_{ij}:	Strain tensor
σ_{ij}:	Stress tensor
ω:	Frequency, eigenvalue
Ω:	Rotating speed
$f(\xi)$:	Shape functions
$[N]$:	Matrix of the shape functions
p:	Number of the shape functions or number of hierarchical terms
t:	Time

E_c: Kinetic energy
E_d: Strain energy
$\{q_i\}$: Generalised coordinates, with $(i = U, V, W, \beta_x, \beta_y, \phi)$
$[M]$: Masse matrix
$[K]$: Stiffness matrix
$[G]$: Gyroscopic matrix.

REFERENCES

[1] H. Zinberg and M. F. Symonds, "The development of an advanced composite tail rotor driveshaft," in *Proceedings of the 26th Annual Forum of the American Helicopter Society*, Washington, DC, USA, June 1970.

[2] H. L. M. dos Reis, R. B. Goldman, and P. H. Verstrate, "Thin-walled laminated composite cylindrical tubes—part III: critical speed analysis," *Journal of Composites Technology and Research*, vol. 9, no. 2, pp. 58–62, 1987.

[3] K. Gupta and S. E. Singh, "Dynamics of composite rotors," in *Proceedings of the Indo-US Symposium on Emerging Trends in Vibration and Noise Engineering*, pp. 59–70, New Delhi, India, March 1996.

[4] C. D. Kim and C. W. Bert, "Critical speed analysis of laminated composite, hollow drive shafts," *Composites Engineering*, vol. 3, pp. 633–643, 1993.

[5] C. W. Bert and C. D. Kim, "Dynamic instability of composite-material drive shaft subjected to fluctuating torque and/or rotational speed," *Dynamics and Stability of Systems*, vol. 10, no. 2, pp. 125–147, 1995.

[6] M.-Y. Chang, J.-K. Chen, and C.-Y. Chang, "A simple spinning laminated composite shaft model," *International Journal of Solids and Structures*, vol. 41, no. 3-4, pp. 637–662, 2004.

[7] C.-Y. Chang, M.-Y. Chang, and J. H. Huang, "Vibration analysis of rotating composite shafts containing randomly oriented reinforcements," *Composite Structures*, vol. 63, no. 1, pp. 21–32, 2004.

[8] S. P. Singh, *Some studies on dynamics of composite shafts*, Ph.D. thesis, Mechanical Engineering Department, IIT, Delhi, India, 1992.

[9] S. P. Singh and K. Gupta, "Dynamic analysis of composite rotors," in *Proceedings of the 5th International Symposium on Rotating Machinery (ISROMAC '94)*, pp. 204–219, Kaanapali, Hawaii, USA, May 1994.

[10] S. P. Singh and K. Gupta, "Dynamic analysis of composite rotors," *International Journal of Rotating Machinery*, vol. 2, no. 3, pp. 179–186, 1996.

[11] S. E. Singh and K. Gupta, "Experimental studies on composite shafts," in *Proceedings of the International Conference on Advances in Mechanical Engineering*, pp. 1205–1221, Bangalore, India, December 1995.

[12] S. P. Singh and K. Gupta, "Composite shaft rotordynamic analysis using a layerwise theory," *Journal of Sound and Vibration*, vol. 191, no. 5, pp. 739–756, 1996.

[13] I. Babuska, B. A. Szabó, and I. N. Katz, "The p-version of the finite element method," *SIAM Journal on Numerical Analysis*, vol. 18, no. 3, pp. 515–545, 1981.

[14] B. A. Szabó and G. J. Sahrmann, "Hierarchic plate and shell models based on p-extension," *International Journal for Numerical Methods in Engineering*, vol. 26, no. 8, pp. 1855–1881, 1988.

[15] B. A. Szabó and I. Babuska, *Finite Element Analysis*, John Wiley & Sons, New York, NY, USA, 1991.

[16] L. Meirovitch and H. Baruh, "On the inclusion principle for the hierarchical finite element method," *International Journal for Numerical Methods in Engineering*, vol. 19, no. 2, pp. 281–291, 1983.

[17] D. C. Zhu, "Development of hierarchical finite element method at BIAA," in *Proceedings of the International Conference on Computational Mechanics*, pp. 123–128, Tokyo, Japan, May 1986.

[18] N. S. Bardell, "The application of symbolic computing to the hierarchical finite element method," *International Journal for Numerical Methods in Engineering*, vol. 28, no. 5, pp. 1181–1204, 1989.

[19] A. Côté and F. Charron, "On the selection of p-version shape functions for plate vibration problems," *Computers & Structures*, vol. 79, no. 1, pp. 119–130, 2001.

[20] A. Houmat, "A sector fourier p-element applied to free vibration analysis of sectorial plates," *Journal of Sound and Vibration*, vol. 243, no. 2, pp. 269–282, 2001.

[21] S. M. Hamza Cherif, "Free vibration analysis of rotating flexible beams by using the fourier p- version of the finite element," *International Journal of Computational Methods*, vol. 2, no. 2, pp. 255–269, 2005.

[22] C. W. Bert and C.-D. Kim, "Whirling of composite-material driveshafts including bending-twisting coupling and transverse shear deformation," *Journal of Vibration and Acoustics*, vol. 117, no. 1, pp. 17–21, 1995.

[23] C. W. Bert, "The effect of bending-twisting coupling on the critical speed of a driveshafts," in *Proceedings of the 6th Japan-US Conference on Composites Materials*, pp. 29–36, Technomic, Orlando, Fla, USA, June 1992.